ELSEVIER

Surface Science 506 (2002) 33–46

SURFACE SCIENCE

www.elsevier.com/locate/susc

Epitaxial growth and interfacial structure of Sn on Si(1 1 1)-(7 × 7)

B. Roldan Cuenya *, M. Doi [1], W. Keune

Laboratorium für Angewandte Physik, FB 10 Physik Gerhard-Mercator-Universität, D-47048 Duisburg, Germany

Received 19 July 2001; accepted for publication 2 October 2001

Abstract

Room temperature stabilization of up to 3.5 ML epitaxial metastable α-Sn at the Si(1 1 1)-(7 × 7) surface is reported. The α-Sn layers remain stabilized at the interface even after the deposition of thick Sn layers that undergo the α-Sn → β-Sn transformation. Additionally, a small decrease in the s-electron density at the ^{119}Sn nucleus is found for submonolayer of Sn at the Sn/Si(1 1 1)-(7 × 7) interface. The epitaxial relationship between thick β-Sn layers on Si(1 1 1) is also shown. The results were obtained by low and high energy electron diffraction and ^{119}Sn conversion electron Mössbauer spectroscopy.

Keywords: Tin; Epitaxy; Growth; Silicon; Low energy electron diffraction (LEED); Reflection high-energy electron diffraction (RHEED); Mössbauer spectroscopy; Metal–semiconductor interfaces

1. Introduction

Bulk Sn is an element that undergoes a phase transformation at 13.2 °C upon cooling from its metallic body centered tetragonal phase (β-Sn, lattice parameters $a = 5.83$ Å, $c = 3.18$ Å) to a semiconducting phase (α-Sn, $a = 6.489$ Å) with diamond structure. α-Sn is interesting for infrared applications because of its nearly zero energy band gap (0.08 eV at room temperature, RT) [1].

Since the discovery of the semiconducting properties of α-Sn in 1950 [1], several groups have tried to grow macroscopic α-Sn crystals [2,3]. The first heteroepitaxial growth of metastable α-Sn films stabilized at RT on closely lattice matched substrates such as InSb ($a = 6.4798$ Å at RT) or CdTe ($a = 6.4829$ Å at RT) was achieved by Farrow et al. [4]. Osaka and co-workers [5] showed that the symmetry of the substrate surface plays a very important role in the determination of the interfacial energy, and that the formation of the β-Sn phase (which is more stable in the bulk at RT than the bulk α-phase) can be inhibited by heteroepitaxy of Sn thin films (<10 Å) on appropriate substrates. Though the α-Sn → β-Sn transformation was observed during heating of epitaxial α-Sn on InSb(0 0 1) at 115 °C [5], the stabilization of α-Sn up to 170° on InSb(1 1 1) [5] was found to be possible, and melting occurred at such high temperature without a phase transformation to β-Sn. For large film thicknesses (>10 Å) [6,7], the

* Corresponding author. Tel.: +49-203-379-2384; fax: +49-203-379-3601.

E-mail address: roldan@uni-duisburg.de (B. Roldan Cuenya).

[1] Permanent address: Department of Materials Science and Engineering, Nagoya University, Nagoya 464-01, Japan.

0039-6028/01/$ - see front matter
PII: S0039-6028(01)01662-4

formation of (bulk-like) β-Sn will be favored, because the free energy of the bulk Sn phase will be lower than the interfacial free energy that stabilizes epitaxial α-Sn.

Sn/Si(1 1 1) is an example of an abrupt metal–semiconductor interface, uncomplicated by interdiffusion or chemical reaction (no silicide formation), that can be used to understand the details of the origin of the Schottky barrier [8]. For instance, it is known from the literature [9] that the difference in the Schottky barrier heights of two different surface phases of Pb/Si(1 1 1) is due to the correlation between the geometric and electronic structure in these systems. A detailed knowledge of the structural properties of the Sn/Si(1 1 1) system is then a requirement for the understanding of its electronic properties.

The growth of epitaxial α-Sn on Si ($a = 5.43$ Å) [6,7,10–13] is difficult due to the large lattice mismatch (~19.5%); for β-Sn on Si the mismatch is 7.4%. Since growth of both, α-Sn and β-Sn is unfavorable on Si(1 1 1), it is not clear in which crystalline form Sn films will grow. Wang et al. [6] studied the growth of Sn on Si(1 1 1) with Sn-($\sqrt{3} \times \sqrt{3}$)R30° and Sn-($2\sqrt{3} \times 2\sqrt{3}$)R30° reconstructions by means of low energy electron diffraction (LEED) and scanning tunneling miscroscopy (STM); they observed that up to 3.5 monolayers (ML) α-like-Sn formed an ordered overlayer commensurable to the Si substrate, which, however, is unstable for larger thicknesses, where β-Sn islands were observed.

The structure of Sn at the *buried* Sn/Si interface is still an open question. It is not known whether interfacial α-like-Sn remains stabilized after the deposition of thicker Sn layers that undergo the transition to β-Sn. The purpose of the present work was to clarify this question. LEED and reflection high energy electron diffraction (RHEED) performed during the growth of Sn on the Si(1 1 1)-(7 × 7) surface will show that ultrathin α-Sn layers are formed. It will be demonstrated by ^{119}Sn conversion electron Mössbauer spectroscopy (CEMS) that these layers remain stabilized as buried α-Sn at the interface up to ~3.5 ML after further coverage by thick β-Sn layers. Moreover, the epitaxial relationship between thick β-Sn layers on Si(1 1 1) is reported.

2. Experimental

Thin epitaxial Sn layers of natural isotopic composition (of 99.995 at.% purity) and ^{119}Sn enriched epitaxial Sn layers, were grown at RT in UHV on the (7 × 7) reconstructed clean Si(1 1 1). The isotopic enrichment of ^{119}Sn was 82.9%.

Before being loaded into the UHV system (base pressure 8×10^{-11} mbar), the Si substrates were rinsed in acetone and ethanol. The (7 × 7)-reconstructed substrate surface was obtained after in situ annealing in UHV at 1100 °C for 15 min to eliminate the top SiO_2 layers. Auger electron spectroscopy (AES) measurements after the in situ cleaning showed a Si surface free of oxygen and carbon contaminants.

Sn layers with thicknesses (t_{Sn}) between 2 and 1000 Å were evaporated from Knudsen-cells (Al_2O_3 crucible) with low deposition rates (0.02–0.025 Å/s). The deposition rates were controlled by a quartz crystal microbalance, which was calibrated by RHEED intensity oscillations observed during quasi-layer-by-layer growth of ultrathin Fe films on Cu(0 0 1) [14]. The pressure during the evaporation was always lower than 5×10^{-10} mbar. To avoid oxidation of the Sn layers during the ex situ measurements, all samples were covered with a 50–60 Å thick amorphous Si layer deposited from an e-gun, before removing them from the UHV system.

For the structural characterization, RHEED measurements were carried out during deposition. The RHEED patterns were recorded by a CCD camera connected to a computerized data storage and processing system [14].

The thickness dependent α- to β-Sn phase transition was also studied ex situ by ^{119}Sn CEMS at RT. For the 23.88 keV Mössbauer γ-radiation, $^{119}Sn^*$ in a $CaSnO_3$ matrix was used as source. For electron detection a He-4% CH_4 gas proportional counter was used, with the sample mounted inside of the counter. An electromechanical Mössbauer drive and conventional electronics were employed, the source being moved in constant acceleration mode. All isomer shift (δ) values are given relative to a $CaSnO_3$ absorber at RT. The Mössbauer spectra were least-squares fitted with the program NORMOS [15] with a Lorentzian line shape.

3. Results

3.1. Reflection high energy electron diffraction

Fig. 1 displays RHEED patterns recorded during growth along the [1 1 2] azimuthal direction of the clean Si(1 1 1)-(7 × 7) surface (a), and the Sn covered Si(1 1 1)-(7 × 7) surface (b)–(d). All images are taken with a low electron beam voltage (6 keV) and a low beam current (25 μA) to avoid heating of the sample surface by the electron beam. The sharpness of the superstructure streaks (six vertical streaks between the central (0,0) and the fundamental (1,1) or $(\bar{1},\bar{1})$ reflection) observed in Fig. 1(a), and the presence of superstructure reflections along several Laue circles, together with the appearance of Kikuchi lines, indicate atomically smooth and well-ordered surfaces. In the same way, sharp fundamental (0,0), (1,1) and $(\bar{1},\bar{1})$ reflections were found after the deposition of 6.8 ML Sn (Fig. 1(d)) demonstrating the flatness of the epitaxial layers.

The growth was observed to be epitaxial and nearly layer-by-layer up to a thickness of 3–3.5 ML (Fig. 1(b) and (c)). The intensity of the fundamental RHEED reflections initially decreases with increasing film thickness (Fig. 1(c)), reaching a minimum at around 3.5 ML. Above this critical thickness, lattice relaxation starts, and the RHEED pattern becomes brighter again. Finally, after depositing 6.8 ML Sn (Fig. 1(d)), a clear increase in the separation of the (1,1) and $(\bar{1},\bar{1})$ RHEED reflections as compared to that of the Si substrate was observed, implying a contraction of the in-plane atomic distance in real space (see also Fig. 3(b) below). This fact can be understood if one considers that for thick Sn layers the more stable phase would be the bulk β-Sn phase, which has a smaller lattice parameter than α-Sn. Therefore, the higher lattice mismatch between substrate and deposited material observed above 3.5 ML appears to be related to the α → β-Sn transition. A change in the structure of the film from diamond (α-Sn) to body-centered tetragonal (β-Sn) can explain the end of the pseudomorphic growth of Sn on the silicon substrate with diamond structure above 3.5 ML.

After deposition of 30 Å Sn, a (1 × 1) RHEED pattern was observed that is characterized by sharp (1,1) and $(\bar{1},\bar{1})$ fundamental streaks, together with weaker (2,2) and $(\bar{2},\bar{2})$ reflections. This indicates good epitaxial quality and good surface flatness of the β-Sn film grown on the interfacial α-Sn layer. Thicker Sn films between 100 Å

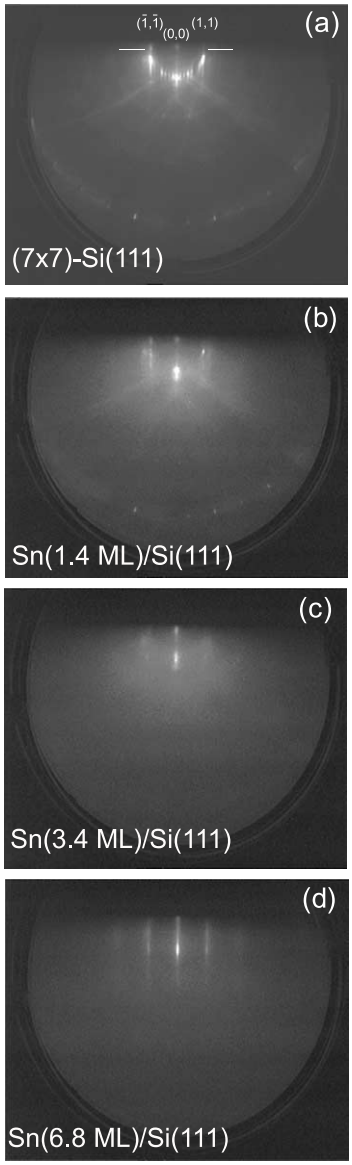

Fig. 1. RHEED patterns recorded along the [1 1 2] azimuthal substrate direction with 6 keV electron energy and 25 μA beam current: (a) (7 × 7) reconstruction of the clean Si(1 1 1) surface immediately prior to deposition; and after deposition of 1.4 ML Sn (b); 3.4 ML Sn (c), and 6.8 ML Sn (d).

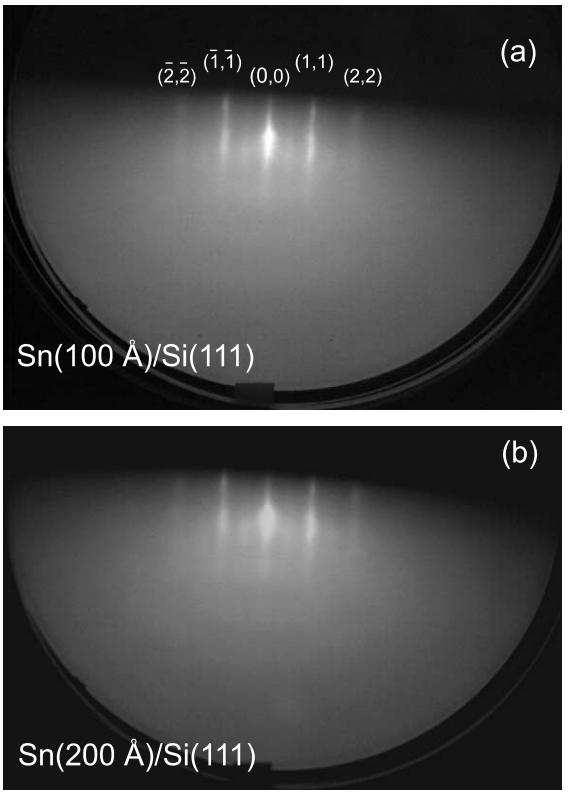

Fig. 2. RHEED patterns recorded along the [1 1 2] azimuthal substrate direction with 10 keV electron energy and 30 μA beam current after deposition of (a) 100 Å Sn and (b) 200 Å Sn on Si(1 1 1).

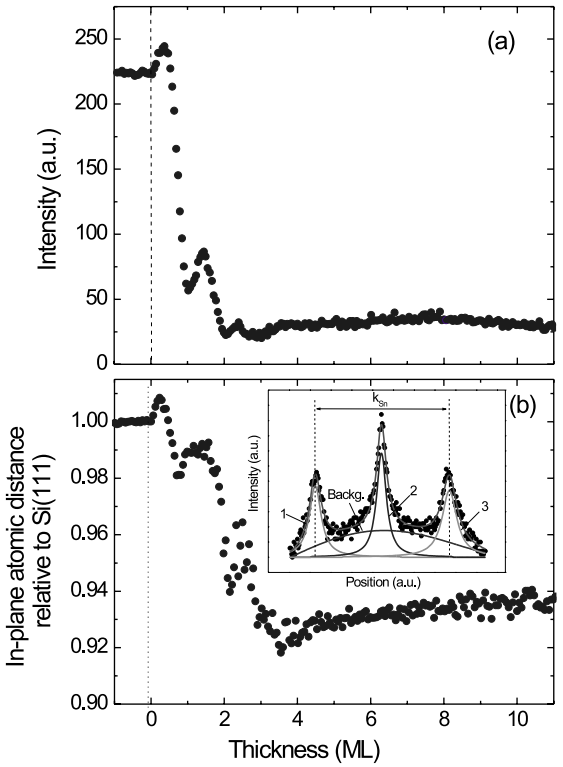

Fig. 3. (a) RHEED intensity (diffuse scattering region along the (0,0) streak) versus Sn thickness; (b) thickness dependence of the Sn in-plane atomic distance relative to that of Si(1 1 1). Insert: intensity profile obtained for 6 ML Sn thickness from the horizontal scan indicated in Fig. 1(a) and fitted with three Lorentzian lines and a parabolic background. (The electron beam was along the [1 1 2] azimuthal substrate direction.)

(Fig. 2(a)) and 200 Å (Fig. 2(b)) still showed relatively long and sharp RHEED streaks, and a weak twofold surface reconstruction appeared. The absence of a spotty pattern in RHEED (that would indicate 3D-islands growth) observed after the deposition of thick Sn layers demonstrates that the growth of Sn occurs with a very flat surface. The Si surface is partially covered by large, flat islands of β-Sn.

The evolution of the RHEED intensity during growth was measured between the (0,0) specular reflection and the shadow-edge (along the (0,0) streak in the region of diffuse scattering [14]). Fig. 3(a) shows that immediately after opening the shutter, the intensity first increases to a maximum and then reaches a minimum at 1 ML thickness as expected under diffuse scattering conditions and layer-by-layer growth. Such intensity oscillations are observed up to 3 ML coverage. The observation of intensity oscillations by RHEED provides evidence for quasi-layer-by-layer growth for the first 3 ML. Above this thickness, the intensity changes only weakly, and no more oscillations are found. The periodicity of the RHEED oscillations corresponds to the thickness of 1 ML α-Sn that experienced a ~9% expansion in the out-of-plane atomic distance along the [1 1 1]-α-Sn direction, as measured with the quartz microbalance during the evaporation. This effect is correlated with the contraction of the in-plane spacing that the interfacial α-Sn experiences to match the in-plane atomic distance of the silicon substrate.

The intensity profiles obtained for different thicknesses from the horizontal scan (as indicated in Fig. 1(a) by the horizontal lines) were fitted with three Lorentzian lines (one for each intensity peak found at the positions, where the fundamental reflections $(\bar{1},\bar{1})$, (0,0) and (1,1) were observed) and a parabolic background. A typical example is shown in the insert of Fig. 3(b). The distance (k_{Sn}) between the $(\bar{1},\bar{1})$ and (1,1) RHEED streaks in reciprocal space is a measure of the Sn in-plane atomic distance ($d_{Sn//}$) in real space (perpendicular to the scattering plane) relative to that of the Si(1 1 1) substrate ($d_{Si//}$):

$$\frac{d_{Sn//}}{d_{Si//}} = \frac{k_{Si}}{k_{Sn}}. \quad (1)$$

The thickness dependence of the relative in-plane atomic distance (Fig. 3(b)) obtained from Eq. (1) also shows three oscillations, correlated with the quasi-layer-by-layer growth of the first three atomic layers (Fig. 3(a)). Oscillations of the in-plane atomic distance were reported in Ref. [16] for Co on Cu(0 0 1) and in Ref. [14] for Fe on Cu(0 0 1). This phenomenon was explained by in-plane atomic distance variations during the nucleation and growth process of monolayer high steps (islands) during this quasi-layer-by-layer growth [16]. In Fig. 3(a), the relative in-plane atomic distance decreases up to 3.5 ML coverage, and above this thickness it approaches a constant value of ~0.93–0.94 (at 12 ML). The critical thickness of 3.5 ML defines the boundary between the α- and β-Sn phases. Experiments performed under similar conditions yield $d_{\beta\text{-}Sn//}/d_{Si//} \sim 0.89$–$0.90$ after the epitaxial growth of 60 Å β-Sn.

Ex situ X-ray diffraction measurements on a 1020 Å thick (bulk-like) β-Sn film epitaxially grown on Si(1 1 1)-(7 × 7) [17] indicated a preferential growth with (2 0 0) lattice planes parallel to the film surface, and with an out-of-plane lattice parameter of 5.825 Å ($a = 5.83$ Å corresponds to bulk β-Sn). This provides information about the relative orientation of the β-Sn bct unit cell grown on the diamond structure of α-Sn/Si(1 1 1): the c-axis is lying within the film plane. The rectangular in-plane unit mesh of β-Sn then should have $a = 5.83$ Å and $c = 3.18$ Å as lattice parameters.

Fig. 4 shows schematically the proposed epitaxial relationship of β-Sn/Si(1 1 1). At first, it is assumed that the (7 × 7) surface reconstruction disappears upon covering by Sn [7], and that the β-Sn overlayer is undistorted, with a bulk unit mesh of dimensions $a = 5.83$ Å and $c = 3.18$ Å in the film plane. Since the bct structure of β-Sn has no threefold rotational axis, the epitaxial growth of the β-Sn unit mesh and the Si(1 1 1) surface as observed by RHEED, as well as the hexagonal symmetry observed in the LEED patterns (as shown in the next section), can be explained by a type of growth similar to Nishiyama–Wassermann growth [18], that explains the epitaxial growth of bcc-Fe(1 1 0) on fcc(1 1 1) or hcp(1 1 1) surfaces.

The suggested β-Sn(2 0 0)/Si(1 1 1) epitaxial relationship displayed in Fig. 4 is applicable to our case, where β-Sn was grown on an epitaxial ultrathin interfacial α-Sn film on Si(1 1 1), because this interfacial α-Sn buffer layer experiences a strong in-plane contraction (Fig. 3(b)) during the

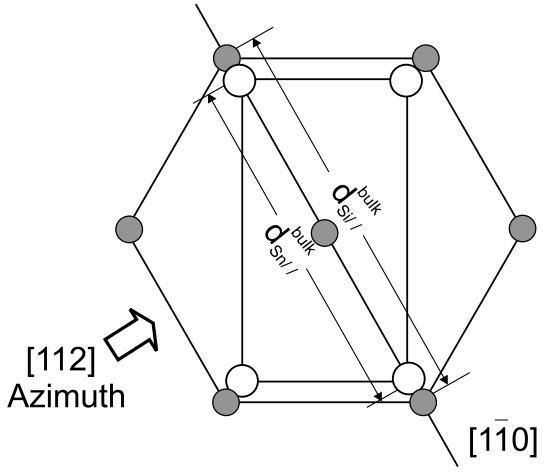

Fig. 4. Schematic model of the epitaxial relationship of β-Sn on the Si(1 1 1) surface, where the full circles represent Si atoms, and the open circles β-Sn adatoms. The 5.83 Å × 3.18 Å rectangular unit mesh ((2 0 0) plane) of unrelaxed (bulk-like) β-Sn is plotted inside the unit mesh of Si(1 1 1). The arrow indicates the incident direction of the electron-beam, i.e. the [1 1 2] direction of the substrate. $d^{bulk}_{Sn//}$ and $d^{bulk}_{Si//}$ are the in-plane atomic distances (perpendicular to the [1 1 2] substrate direction) of undistorted β-Sn and Si(1 1 1), respectively. The Sn unit cell of only one type of crystallographic domains is shown. Equivalent crystallographic domains of β-Sn(2 0 0) grow with their unit cells rotated by ±60° in the film plane.

initial growth stage to match the smaller lattice parameter of Si. Following this epitaxial model, the in-plane atomic distance $d^{bulk}_{Sn//}$ of undistorted bulk-like β-Sn observed perpendicular to the [1 1 2] azimuthal substrate direction should be smaller than that of Si(1 1 1), $d^{bulk}_{Si//}$. This is qualitatively in accordance with the RHEED result above 3.5 ML (Fig. 3(b)), where a 6–7% contraction of the in-plane atomic spacing of Sn is measured. An even larger in-plane contraction (~11%) was measured by RHEED for thicker Sn films (60 Å) deposited under similar conditions (not shown). Quantitatively, following this growth model (Fig. 4), the relative in-plane atomic distance, $d^{bulk}_{Sn//}/d^{bulk}_{Si//}$, of unstrained (bulk-like) β-Sn is expected to be 0.87, which should be compared with the value of $d_{Sn//}/d_{Si//} \sim 0.90$–$0.94$ measured by RHEED. The difference between these values demonstrates that in reality the epitaxial β-Sn(2 0 0) layers are in-plane expanded by 3–7% along the [1 $\bar{1}$ 0] direction, as compared with the case of bulk β-Sn.

3.2. Low energy electron diffraction

Fig. 5(a) shows a typical LEED pattern of the atomically clean Si(1 1 1)-(7 × 7) surface measured at RT with an incident electron energy of 76 eV. With the same energy and same azimuthal orientation, but after the deposition of 60 Å Sn, LEED images were recorded at RT (Fig. 5(b)) and −115 °C (Fig. 5(c)). The schematics of the arrangement of the LEED spots after the deposition of 60 Å Sn are plotted in Fig. 5(b) and (c) (right-hand side).

At RT (Fig. 5(b)), a (1 × 1) hexagonal pattern with the same dimensions and orientation as the Si(1 1 1) substrate is observed. The sharpness of these spots and their circular shape also suggest that they originate from a well ordered surface, such as the substrate. This observation supports the idea of island growth, with substrate regions almost uncovered and other regions covered by flat Sn islands. No LEED spots of α-Sn or β-Sn can be observed at RT at 76 eV. The lack of β-Sn reflections in LEED at RT after the deposition of 60 Å Sn, in spite of the good epitaxial quality of up to 200 Å thick Sn layers according to RHEED (see Fig. 2(b)), is explained by the very small Debye–Waller factor of β-Sn ($f_\beta = 0.042$ [19]). With decreasing temperature, the Debye–Waller factor is known to increase strongly. In fact, f_β increases, and at a temperature of −115 °C, additional reflections with larger inverse spacing (smaller atomic distance) than the Si substrate, but with the same azimuthal orientation, appear in the LEED pattern (Fig. 5(c)). These reflections which are clearly observed for energies between 70–80 eV are attributed to β-Sn. This result is in accordance with our epitaxial model plotted in Fig. 4. The LEED spots related to β-Sn are circularly elongated. This shows that the β-Sn domains (according to Fig. 4) have a crystallographic texture in the film plane, with a small distribution of azimuthal twisting angles within 10–15°.

Using the Si(1 1 1) substrate as reference, the LEED measurements show that the ratio of the atomic distances along the [1 $\bar{1}$ 0] direction, i.e. $d_{Sn//}/d_{Si//} \approx 0.89$, is compatible with the ratio for the bulk atomic distances $d^{bulk}_{Sn//}/d^{bulk}_{Si//} \approx 0.87$ (see Fig. 4), if a ≈ 2.3% in-plane expansion of β-Sn along [1 $\bar{1}$ 0] is taken into account. The in-plane atomic distance measured by RHEED along the same direction (see Fig. 3(b)) also points at an in-plane expansion of the β-Sn films, though the measured expansion is larger (3–7%).

At higher electron energies (85–110 eV), an additional pattern with circularly elongated spots, hexagonal symmetry, and rotated by 30° with respect to the pattern of the Si substrate can be observed at RT for Sn thicknesses up to 100 Å. Fig. 6(a) displays a LEED pattern of the atomically clean Si(1 1 1)-(7 × 7) surface measured at RT with an energy of 95 eV. With the same angular geometry and energy as in Fig. 6(a), but after the deposition of 60 Å Sn, LEED images were recorded with the sample maintained at RT (Fig. 6(b)) and at −115°C (Fig. 6(c)). The schematics of the spot arrangement observed in LEED are again plotted on the right. At RT (Fig. 6(b)), the weak spots from the fundamental (1 × 1) pattern of the substrate appear, together with a new hexagonal pattern with circularly elongated spots that is rotated by 30° with respect to the Si(1 1 1)-(1 × 1) pattern. The new rotated pattern observed presents the same in-plane atomic distance as the substrate, and since it can be observed at RT and low temperature, it cannot be attributed to β-Sn.

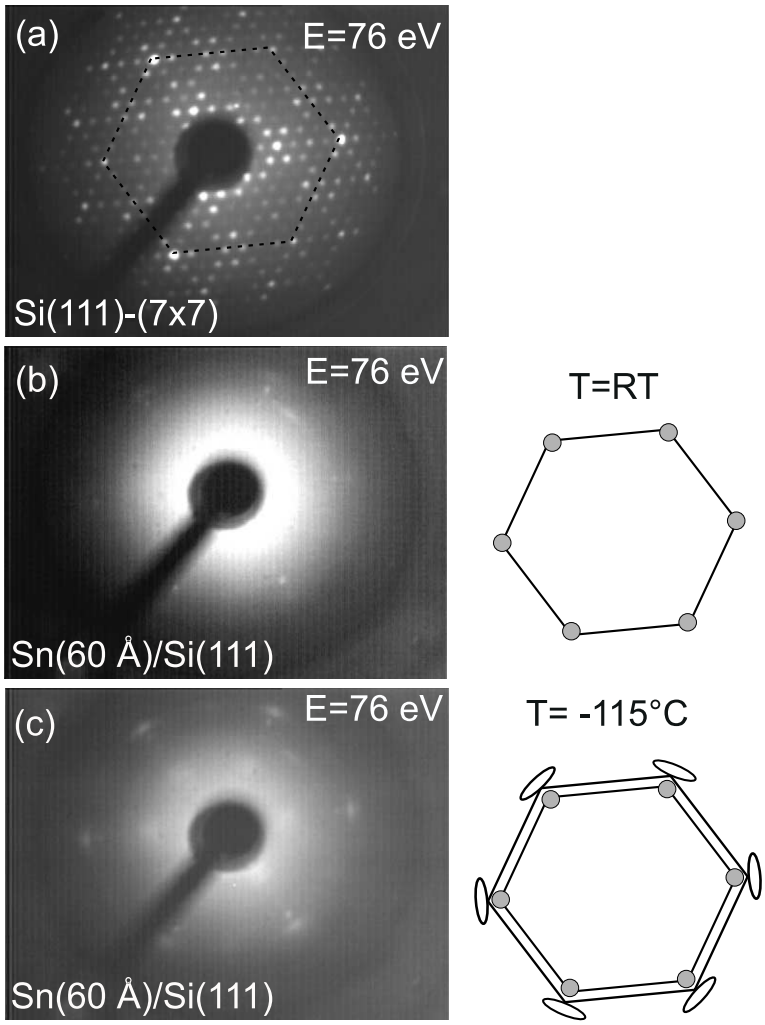

Fig. 5. LEED patterns of the atomically clean Si(1 1 1)-(7 × 7) surface measured at RT (a) and of 60 Å Sn epitaxially grown on Si(1 1 1)-(7 × 7) measured at RT (b) and at −115 °C (c), together with schematics of the arrangement of reflections observed (right). All images have been taken under the same angular geometry, and the distances of camera and sample to the LEED screen have been maintained constant. The incident electron energy was 76 eV. The weak circular sharp spots (shaded circles) in (b) and (c) originate from the Si substrate, while the elongated spots (open ellipses) in (c) originate from the epitaxial β-Sn overlayer.

(The LEED pattern from β-Sn at RT is too weak to be observed due to the low Debye–Waller factor). Therefore, the rotated pattern presumably originate from substrate regions covered by only small amounts of Sn that remain stabilized as α-like-Sn constrained by the Si substrate. These areas can be detected by LEED at RT because of the larger Debye–Waller factor ($f_\alpha = 0.16$) of α-Sn relative to that of the β-Sn phase ($f_\beta = 0.042$). The 30° rotation observed is not unusual, as it is well known [7,20] that submonolayer Sn films tend to form surface reconstructions that are rotated by 30° with respect to the diffraction pattern of the substrate. Similar LEED patterns with hexagonal symmetry and almost identical in-plane unit-mesh to the substrate, but rotated by 30°, have been recorded at RT also for total Sn thicknesses of 20, 30 and 100 Å (not shown).

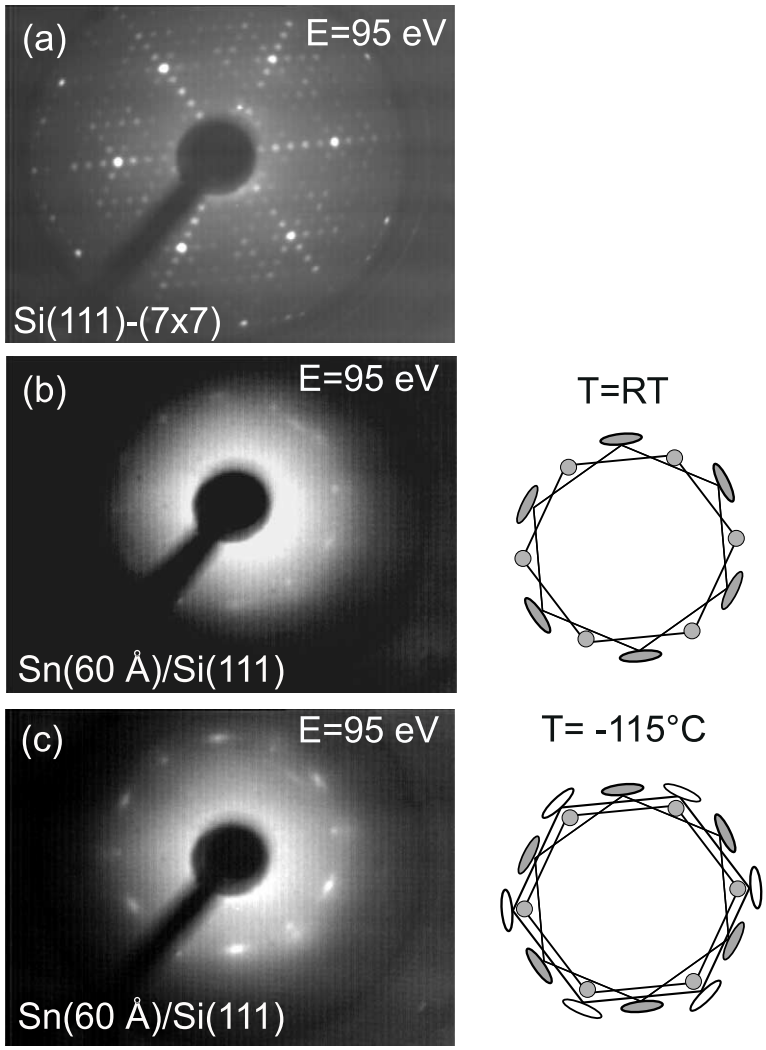

Fig. 6. LEED patterns of the atomically clean Si(1 1 1)-(7 × 7) surface measured at RT (a) and of 60 Å Sn epitaxially grown on Si(1 1 1)-(7 × 7) measured at RT (b) and at −115 °C (c), together with a schematics of the arrangement of reflections observed (right). All images have been taken under the same angular geometry, and the distances of camera and sample to the LEED screen have been maintained constant. The incident electron energy was 95 eV. Shaded circles: weak spots from Si substrate; open ellipses: reflections from β-Sn. An additional hexagonal pattern (dark ellipses) rotated by 30° with respect to that of the Si(1 1 1) substrate appears in (b) and (c).

Fig. 6(c) shows a LEED pattern of 60 Å Sn deposited on Si(1 1 1) and measured at −115°C ($E = 95$ eV). In this case, together with the two sets of reflections from the Si substrate and presumably 30°-rotated α-Sn, very weak β-Sn spots (hardly visible in Fig. 6(c)), with an in-plane unit mesh larger than the Si substrate in reciprocal space were observed. This β-Sn pattern is similar to that observed in Fig. 5(c) for a lower incident electron energy.

Above 115 eV and up to 200 eV, the LEED patterns observed show only (1 × 1) reflections from the Si(1 1 1) substrate. The spots observed were not elongated or rotated, but rather sharp, showing a threefold symmetry for certain energies which is characteristic of the Si(1 1 1) surface.

Scanning electron microscopy images performed ex situ on Sn(200 Å)/Si(1 1 1) (see Section 3.4) will confirm the hypothesis of the formation of Sn islands that do not coalesce even after the deposition of a large amount of Sn, leaving regions on the substrate between β-Sn islands which are almost uncovered.

3.3. Auger electron spectroscopy

The dependence of AES spectra on Sn film thickness has been measured in order to investigate the origin of the substrate-like (1 × 1) LEED pattern observed on Sn-covered Si(1 1 1). Fig. 7 displays AES spectra measured after the deposition of Sn films of various thicknesses. In addition to the strong double peak of Sn at 430–437 eV, the weaker peak of Si at 91 eV can be observed in all spectra. The intensity of the AES Si signal relative to the Sn signal decreases with increasing Sn thickness (from 10 to 200 Å Sn), but does not vanish (Fig. 8). This demonstrates that there are substrate regions covered only by a small amount of Sn (presumably α-Sn) even after the deposition of relatively thick Sn films, and these open regions provide a non-negligible substrate signal to the LEED patterns.

3.4. Scanning electron microscopy

Scanning electron microscopy measurements were performed ex situ on an uncoated 200 Å thick β-Sn film epitaxially grown on Si(1 1 1)-(7 × 7). Fig. 9(a) and (b) show large Sn islands of diameters between 100–500 nm. The islands do not coalesce even after depositing 200 Å Sn, and regions of the Si substrate almost uncovered by Sn can be observed. This effect must be due to the large surface energy of the β-Sn clusters as compared to the Sn/Si interfacial energy, resulting in agglomeration rather than wetting of the substrate. The rather sharp RHEED streaks (Fig. 2(b)) measured on such samples show that the top surface of the extended Sn islands must be relatively flat on an atomic scale. The island structure explains the non-negligible AES signals (Fig. 8) and (1 × 1) LEED patterns (Figs. 5 and 6), both originating from the Si substrate due to the open substrate regions, even for very thick Sn films.

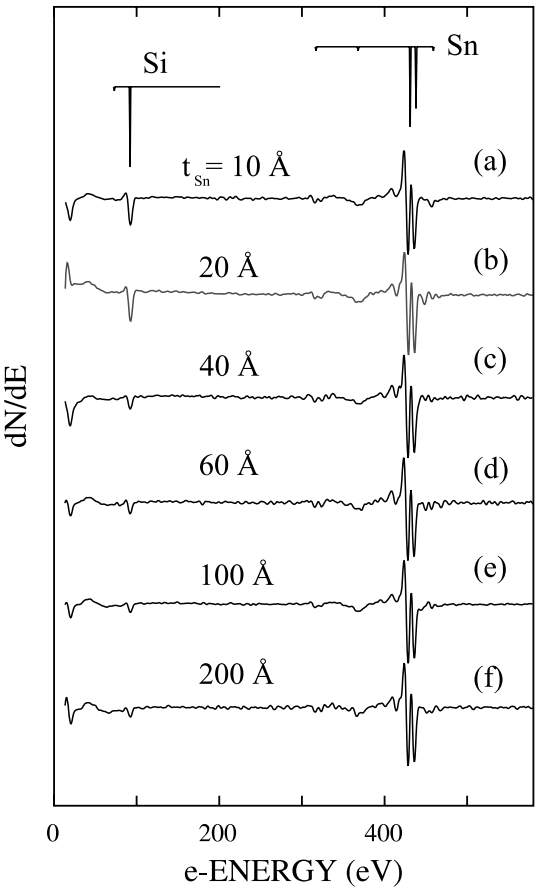

Fig. 7. Auger electron spectra measured after the deposition of Sn(t_{Sn}) on Si(1 1 1)-(7 × 7) with t_{Sn} = 10 Å (a), 20 Å Sn (b), 40 Å (c), 60 Å (d), 100 Å Sn (e), and 200 Å Sn (f). The bar diagrams on top of the spectra indicate the predicted positions of the AES peaks of Si and Sn. For comparison, all spectra have been normalized to show the same peak-to-peak Sn intensity.

3.5. ^{119}Sn conversion electron Mössbauer spectroscopy

It is well known [21,22], that measurements of the isomer shift in thin Sn layers and multilayers enable one to distinguish α- from β-Sn [17,23], taking into account the ≃0.5 mm/s difference in the isomer shifts of bulk α-Sn ($\delta = +2.03 \pm 0.02$ mm/s at RT) and bulk β-Sn ($\delta = +2.56 \pm 0.01$ mm/s at

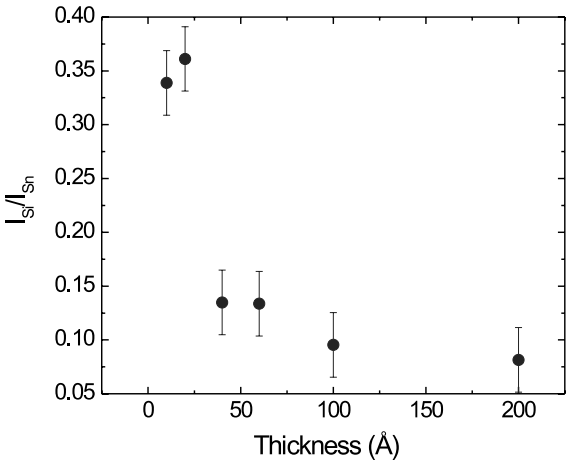

Fig. 8. AES intensity ratio of Si (at 91 eV) and Sn (at 430 eV) signals (measured peak to peak) versus Sn film thickness.

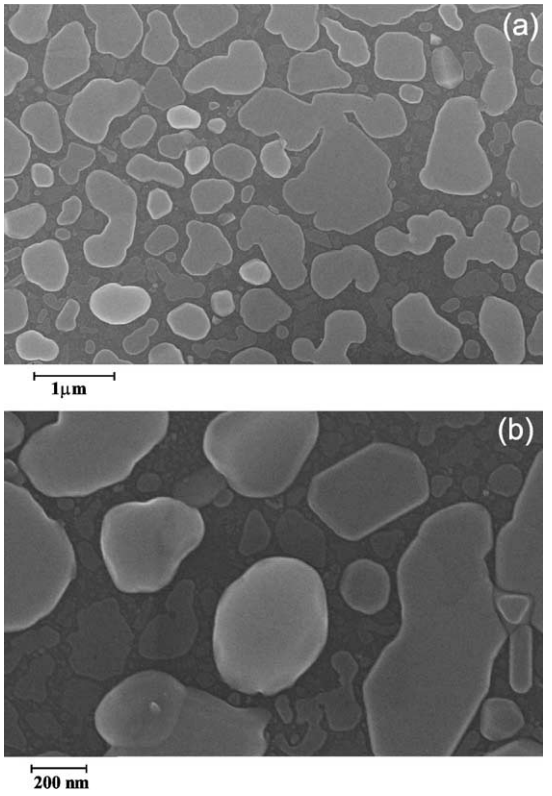

Fig. 9. Ex situ scanning electron microscopy images of epitaxial 200 Å thick Sn film on Si(1 1 1)-(7 × 7) measured with scales of (a) 1 μm and (b) 200 nm.

RT), both values relative to the $BaSnO_3$ (or $CaSnO_3$) standard absorber [21–23].

Fig. 10 displays the thickness dependence of ^{119}Sn CEM spectra of epitaxial Sn layers grown on Si(1 1 1)-(7 × 7) at RT. Below 4 ML coverage (Fig. 10(a)–(c)), pure α-Sn was found. β-Sn appears above this critical thickness when the coverage is

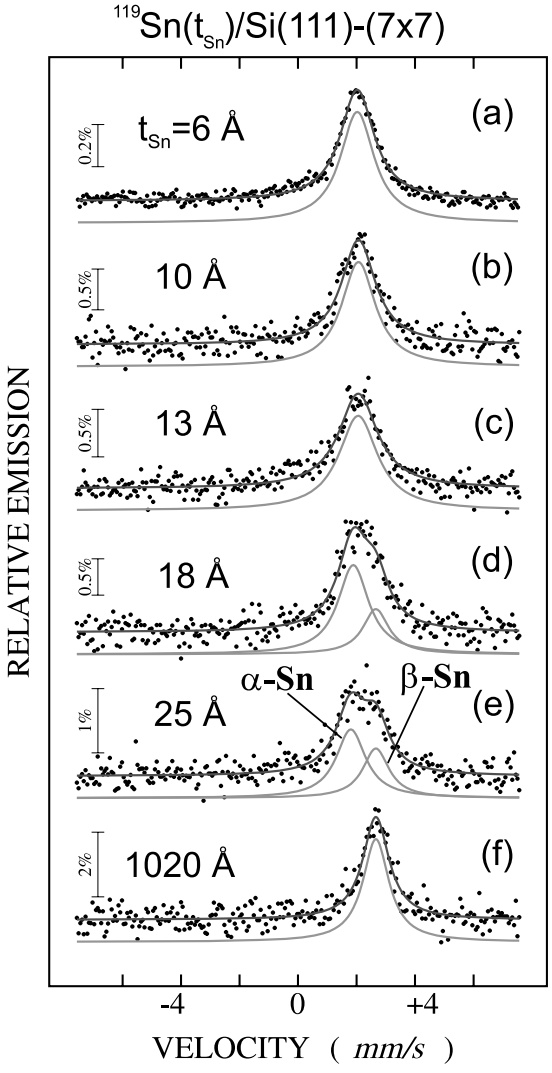

Fig. 10. ^{119}Sn CEM spectra of epitaxial ^{119}Sn(t_{Sn}) on Si(1 1 1)-(7 × 7) deposited and measured (ex situ) at RT: (a) $t_{Sn} = 6$ Å, (b) $t_{Sn} = 10$ Å, (c) $t_{Sn} = 13$ Å, (d) $t_{Sn} = 18$ Å, (e) $t_{Sn} = 25$ Å, (f) $t_{Sn} = 1020$ Å, all samples were coated by 50–60 Å amorphous Si for protection.

further increased (Fig. 10(d),(e)). Fig. 10(f) shows a typical β-Sn spectrum corresponding to approximately 1020 Å natural Sn on Si(1 1 1)-(7 × 7). It is important to note that after the thickness dependent α → β-Sn transition at 3.5–4 ML has occurred, α-Sn remains stabilized at the interface, and does not transform to β-Sn upon further coverage with Sn (Fig. 10(d) and (e)).

Table 1 displays the Mössbauer parameters (isomer shift δ, Lorentzian linewidth Γ, and the relative contribution of the α- and β-Sn phases (A_α, A_β) to the total spectral area of the Mössbauer spectra) obtained by least-squares fitting of the experimental spectra. All spectra were fitted either with one (Fig. 10(a)–(c) and (f)) or two (Fig. 10(d) and (e)) Lorentzian lines. The isomer shifts of these lines are in accordance with those of the α-Sn and β-Sn phases, respectively.

In Fig. 10(f), no α-Sn contribution was detected, because this 1020 Å thick Sn sample is made from natural Sn, and 3.5 ML or ~13 Å of natural α-Sn (being the α-Sn maximum thickness that can be stabilized at the interface) will give an effective Mössbauer signal equivalent to only ~1 Å of ^{119}Sn. This is a negligible signal as compared to that from the residual 1007 Å β-Sn layer.

For a more detailed study of the Sn/Si(1 1 1)-(7 × 7) interface, 0.7–1.5 ML thick isotopically enriched ^{119}Sn probe layers (82.9%) were deposited in several positions directly at and near to the Sn/Si interface. Interface-selectivity is achieved by means of these strategically positioned ^{119}Sn probe layers, which are surrounded by thin natural Sn layers (natural ^{119}Sn abundance: 8.58%).

Fig. 11 displays CEM spectra from the ^{119}Sn probe layers. Since only 8.58% ^{119}Sn is found in natural Sn, the ^{119}Sn CEMS signal originates predominantly from the ^{119}Sn probe layers. The spectra in Fig. 11(b) to (d) exhibit the typical isomer shift of α-Sn (Table 2), independent of the thin natural β-Sn layers. Fig. 11(b) demonstrates that 1.5 ML of α-Sn remains stable at the Sn/Si(1 1 1)-(7 × 7) interface even after depositing another 4.5 ML of natural Sn on top.

Fig. 11(c) displays the CEM spectrum of a 1.5 ML thick ^{119}Sn probe layer that is coated by 4.5 ML of natural Sn and is separated from the Sn/Si(1 1 1) interface by 1.5 ML of natural Sn. Since this probe layer exhibits the isomer shift of α-Sn (Table 2), this result proves that at least the first 3 ML of Sn grown on Si(1 1 1)-(7 × 7) are stabilized in the α-Sn phase.

Finally, Fig. 11(d) and the isomer shift values in Table 2 prove that a submonolayer (0.7 ML) of Sn at the Sn/Si(1 1 1)-(7 × 7) interface remains α-like-Sn after coating with 4 ML of natural Sn, since the measured isomer shift (δ) is close to that of bulk α-Sn. Nevertheless, a slight difference in the isomer shift of this ultrathin layer with respect to that of bulk α-Sn is found. In this case, δ is equal to $+1.90 \pm 0.03$ mm/s, which is slightly smaller than the value for bulk α-Sn (+2.03 mm/s at RT) [22]. This indicates that the electronic structure of such submonolayer interfacial Sn layers is slightly modified.

Table 1
^{119}Sn Mössbauer parameters (isomer shift δ, linewidth Γ) obtained from Fig. 10

Sn(t_{Sn})/Si(1 1 1)	Isomer shift δ (mm/s)		Lorentzian linewidth (FWHM) Γ (mm/s)		Area (%)	
t_{Sn} (Å)	α-Sn	β-Sn	α-Sn	β-Sn	α-Sn (A_α)	β-Sn (A_β)
6	2.023 ± 0.008		1.40 ± 0.03		100 ± 2	
10	2.07 ± 0.02		1.41 ± 0.07		100 ± 4	
13	2.06 ± 0.02		1.61 ± 0.07		100 ± 4	
18	1.89 ± 0.04	2.66	1.3 ± 0.1	1.08	70 ± 8	30 ± 5
25	1.80 ± 0.05	2.66	1.2 ± 0.1	1.08	61 ± 7	39 ± 5
1020		2.66 ± 0.02		1.08 ± 0.06		100 ± 5

For $18 \leqslant t_{Sn} \leqslant 1020$ Å, the isomer shift and linewidth of the β-Sn line was a fixed parameter at +2.66 mm/s during the least-squares fitting, which is the value obtained for 1020 Å β-Sn epitaxially grown on Si(1 1 1). A_α and A_β represent the relative contribution of the α- and β-Sn phases, respectively, to the total spectral area of the Mössbauer spectra.

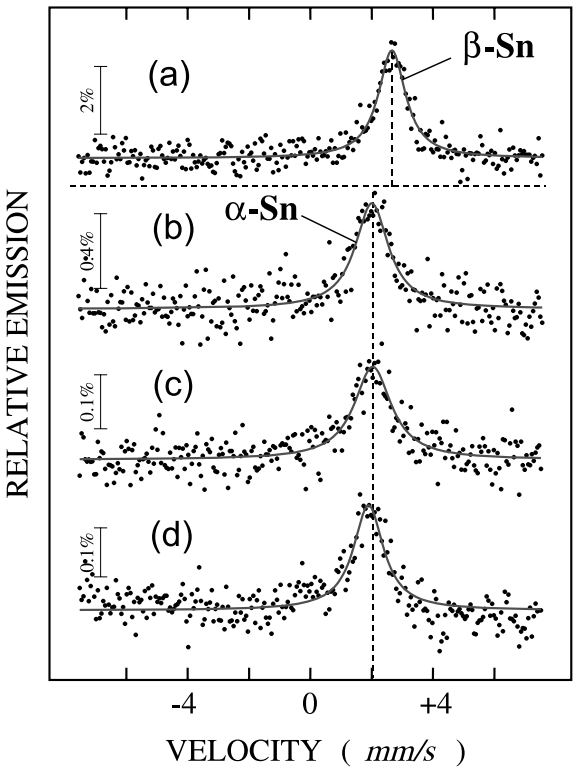

Fig. 11. ^{119}Sn probe-layer CEM spectra measured (ex situ) at RT on epitaxial Sn films on Si(1 1 1)-(7 × 7): (a) ^{nat}Sn(1020 Å)/Si(1 1 1); (b) ^{nat}Sn(4.5 ML)/^{119}Sn(1.5 ML)/Si(1 1 1), (c) ^{nat}Sn(4.5 ML)/^{119}Sn(1.5 ML)/^{nat}Sn(1.5 ML)/Si(1 1 1) and (d) ^{nat}Sn(3.7 ML)/^{119}Sn(0.7 ML)/Si(1 1 1). All samples were coated by 50–60 Å amorphous Si for protection. (^{nat}Sn means Sn of natural isotopic abundance.)

4. Discussion

The α-Sn/Si(1 1 1) interface has a lower misfit energy than the β-Sn/Si(1 1 1) interface, which would have to accommodate a considerable mismatch in symmetry and dimension via interfacial dislocations. The epitaxial growth observed in RHEED (Figs. 1 and 3) up to 3.5 ML shows that the α-Sn/substrate misfit is accommodated largely by misfit elastic strain. This maximum interfacial α-Sn thickness of ~3.5 ML is in agreement with STM studies performed by Wang et al. [6], who observed the onset of β-Sn island growth above 3.5 ML.

The in-plane atomic distances displayed in Fig. 3(b) show that the influence of the substrate on the condensing adatoms diminishes with increasing thickness during growth, and after reaching a critical thickness of 3.5 ML, the nucleation of epitaxial β-Sn during growth at a temperature > 13.2 °C is energetically more favorable than the continuation of the α-Sn growth.

During the experiments the importance of a well ordered and clean Si(1 1 1)-(7 × 7) surface for the α-Sn interfacial stabilization was noticed, because the deposition of Sn on C or O contaminated surfaces promoted the nucleation of β-Sn at an earlier stage of growth (<3.5 ML). Even long time RHEED observations with a high electron beam voltage (>10 keV) during RT deposition were found to affect the local Sn growth [7], because a slight increase in temperature promotes an earlier α- to β-Sn transformation. These facts might explain some of the controversy in the literature. For instance, Ichikawa [7] reports that in RHEED patterns no evidence was found of epitaxial growth of grey Sn layers on Si(1 1 1)-(7 × 7) substrates; however, in the same report it is also claimed that thin layers of grey tin were formed, though poorly, on Si(1 1 1)-(7 × 7) surfaces.

Mössbauer measurements performed on 0.7 ML α-Sn deposited directly at the Si(1 1 1) interface (Fig. 11 and Table 2) indicated $a \sim 0.13$ mm/s decrease $\Delta\delta$ in the isomer shift with respect to the

Table 2
^{119}Sn Mössbauer parameters (isomer shift δ, linewidth Γ) obtained from Fig. 11

Sample	Isomer Shift (δ (mm/s)		Lorentzian linewidth (FWHM) Γ (mm/s)
	α-Sn	β-Sn	
^{nat}Sn(1020 Å)/Si(1 1 1)		2.66 ± 0.02	1.08 ± 0.06
^{nat}Sn(4.5 ML)/^{119}Sn(1.5 ML)/Si(1 1 1)	2.01 ± 0.03		1.3 ± 0.1
^{nat}Sn(4.5 ML)/^{119}Sn(1.5 ML)/^{nat}Sn(1.5 ML)/Si(1 1 1)	2.03 ± 0.04		1.5 ± 0.1
^{nat}Sn(3.7 ML)/^{119}Sn(0.7 ML)/Si(1 1 1)	1.90 ± 0.03		1.19 ± 0.09

value of bulk α-Sn. Since the isomer shift is proportional to the total s-electron density at the nucleus, $|\psi(0)|^2$, the decrease in the isomer shift of interfacial α-Sn obtained is equivalent to a reduction $\Delta|\psi(0)|^2$ of the s-electron density at the Sn nucleus by $\approx 1.5a_0^{-3}$ (a_0 = Bohr radius), relative to bulk α-Sn, as follows from Eq. (2):

$$\Delta|\psi(0)|^2 = \Delta\delta/\alpha, \tag{2}$$

where $\alpha = 0.086a_0^{-3}$ mm/s for ^{119}Sn [24].

This effect indicates some kind of electronic interaction between Sn and Si atoms at the interface. Ichikawa et al. [7] proposed the formation of Sn germanides and Sn silicides in the surface regions as possible explanation for the appearance of new superstructures (e.g. $\sqrt{91} \times \sqrt{3}$, $\sqrt{133} \times 4\sqrt{3}$) during the growth of Sn on Ge(1 1 1) or Si(1 1 1) substrates at high temperatures. Ichikawa affirmed that the large superstructures observed were not the result from adsorption of Sn atoms on special positions (e.g. on-top and hollow sites) of the substrate surface, but were Sn overlayers reconstructed by a deposit–substrate interaction. Such an interaction could also explain the slight reduction of s-electron density at the Sn nuclei that has been observed.

5. Conclusions

The RT epitaxial growth and structure of Sn layers on Si(1 1 1)-(7 × 7) surfaces was investigated by RHEED, LEED and ^{119}Sn CEMS. The formation of up to 3.5 ML of metastable α-Sn at the Sn/Si(1 1 1) interface was observed by CEMS. The interfacial α-like-Sn layer remains stabilized even after further deposition of thick Sn layers that undergo the α-Sn → β-Sn transformation. Layer-by-layer-like growth is observed up to 3 ML coverage, i.e. in the α-Sn region. The growth of α-Sn starts with the in-plane atomic spacing of Si(1 1 1). With increasing coverage (up to 3.5 ML) the in-plane atomic spacing of α-Sn decreases rapidly and shows oscillating behavior that is correlated with quasi-layer-by-layer growth. In the β-Sn region (above ~3.5–4 ML coverage) the in-plane atomic distance remains nearly constant and is found to be expanded by 2–7% relative to that of bulk β-Sn.

In this context it is interesting mentioning that a similar behavior in terms of interfacial α-Sn layer thickness is observed, if one uses an amorphous Si layer as template for the growth of (in this case amorphous) α-like Sn films [17]. It appears that the structure and symmetry of the substrate is irrelevant with respect to the thickness of the α-Sn layer (amorphous or crystalline) that is stabilized by interface free energy terms.

Moreover, the present RHEED and LEED results demonstrate that flat epitaxial β-Sn islands grow for Sn coverages larger than 3.5–4 ML with the epitaxial relationship β-Sn(2 0 0) ‖ Si(1 1 1) and β-Sn[0 1 1] ‖ Si[1 $\bar{1}$ 0]. The observed sixfold LEED pattern is compatible with three crystallographic domains. each with this epitaxial relationship, but rotated relative to each other by 60° and 120° in the film plane. These rotational angles show a small angular distribution in the film plane with a width of 10–15°. AES signals and SEM images demonstrate that the flat β-Sn islands do not uniformly cover the substrate surface even after the deposition of up to 200 Å Sn. Thus, wetting of the Si substrate by Sn is inhibited.

For several incident electron energies (85–110 eV) and rather thick Sn films, an additional sixfold (1 × 1) LEED pattern similar to the fundamental reflections of the Si(1 1 1) substrate, but rotated by 30°, was observed. This pattern might originate from the open space between β-Sn islands, where possibly surface reconstructed ultrathin α-Sn overlayers on Si(1 1 1) with no or little β-Sn coverage exist.

Only a small decrease (relative to bulk α-Sn) by $\sim 1.5a_0^{-3}$ of the total s-electron density at the ^{119}Sn nucleus was measured for submonolayers of ^{119}Sn at the α-Sn/Si(1 1 1) interface, indicating only weak electronic charge transfer at the interface.

Acknowledgements

We are grateful to U. von Hörsten for valuable technical assistance, to W. Kunze for performing the SEM measurements, and to Dr. H. Nienhaus for helpful discussion. This work was supported by the Deutsche Forschungsgemeinschaft (GRK 277).

References

[1] G.A. Busch, R. Kern, Solid State Phys. 11 (1961) 1.
[2] A.W. Ewald, O.N. Tufle, J. Appl. Phys. 29 (1958) 1007.
[3] J.H. Becker, J. Appl. Phys. 29 (1958) 1110.
[4] R.F.C. Farrow, D.S. Robertson, G.M. Williams, A.G. Cullis, G.R. Jones, I.M. Young, P.N.J. Dennis, J. Cryst. Growth 54 (1981) 507.
[5] T. Osaka, H. Omi, K. Yamamoto, A. Ohtake, Phys. Rev. B 50 (1994) 7567.
[6] D.T. Wang, N. Esser, M. Cardona, J. Zegenhagen, Surf. Sci. 343 (1995) 31.
[7] T. Ichikawa, Surf. Sci. 140 (1984) 37.
[8] R.F. Schmitsdorf, T.U. Kampen, W. Mönch, J. Vac. Sci. Tech. B 15 (1997) 1221.
[9] D.R. Heslinga, H.H. Weitering, D.P. van der Werf, T.M. Klapwijk, Phys. Rev. Lett. 64 (1990) 1589.
[10] P.J. Estrup, J. Morrison, Surf. Sci. 2 (1964) 465.
[11] C. Törnevik, M. Hammar, N.G. Nilsson, S.A. Flodström, Phys. Rev. B 44 (1991) 13144.
[12] M.S. Worthington, J.L. Stevens, C.S. Chang, I.S.T. Tsong, Nuclear Instrum. Methods Phys. Res. B 64 (1992) 566.
[13] A.H. Levermann, P.B. Howes, K.A. Edwards, H.T. Anyele, C.C. Matthai, J.E. Macdonald, R. Feidenhans'l, L. Lottermoser, L. Seehofer, G. Falkenberg, R.L. Johnson, Appl. Surf. Sci. 104–105 (1996) 124.
[14] A. Schatz, W. Keune, Surf. Sci. Lett. 440 (1999) L841.
[15] R.A. Brand, Nucl. Instrum. Methods B 28 (1987) 417.
[16] J. Fassbender, U. May, B. Schirmer, R.M. Jungblut, B. Hillebrands, G. Güntherodt, Phys. Rev. Lett. 75 (1995) 4476.
[17] B. Roldan Cuenya, W. Keune, W. Sturhahn, M.Y. Hu, T.S. Toellner, Phys. Rev. B 64 (2001) 235321.
[18] O. Hellwig, K. Theis-Bröhl, G. Wilhelmi, A. Stierle, H. Zabel, Surf. Sci. 398 (1998) 379.
[19] A. Barla, R. Rüffer, A.I. Chumakov, J. Metge, J. Plessel, M.M. Abd-Elmeguid, Phys. Rev. B 61 (2000) R14881.
[20] T. Ichikawa, S. Ino, Surf. Sci. 105 (1981) 395.
[21] A. Svane, N.E. Christensen, C.O. Rodriguez, M. Methfessel, Phys. Rev. B 55 (1997) 12572.
[22] J.G. Stevens, V.E. Stevens (Eds.), Mössbauer Effect Data Index Covering the 1974 Literature, IFI/Plenum, New York, 1975, p. 153.
[23] B. Roldan Cuenya, M. Doi, O. Marks, W. Keune, K. Mibu, P. Entel, D.E. Wolf (Eds.), Structure Dynamics of Heterogeneous Systems, World Scientific, Singapore, 2000, p. 251.
[24] M. Grodzicki, V. Männing, A.X. Trautwein, J.M. Friedt, J. Phys. B: At. Mol. Phys. 20 (1987) 5595.